Applied Catalysis A, General 647 (2022) 118914

Contents lists available at ScienceDirect

Applied Catalysis A, General

journal homepage: www.elsevier.com/locate/apcata

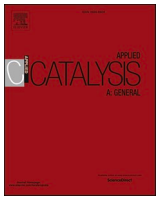

Remarkable stability of Ni-modified polyoxometalates to H_2, CO, and CH_4 during propylene oligomerization

Galiya Magazova, Yoonrae Cho, Jessica A. Muhlenkamp, Jason C. Hicks [*,1]

Department of Chemical and Biomolecular Engineering, University of Notre Dame, 250 Nieuwland Hall, Notre Dame, IN, 46556, United States

ARTICLE INFO

Keywords:
Shale gas
Olefin
Dimerization
Alkene
Nickel
Heterogeneous Catalysis

ABSTRACT

Olefin oligomerization is a crucial step in the synthesis of chemicals and fuels via the formation of higher molecular weight intermediate products. Upstream processes that produce olefin building blocks, however, may contain impurities that affect catalyst performance and process design strategies. Supported Ni-modified Wells–Dawson (WD)-type polyoxometalates (POM) have been reported as active and regenerable olefin oligomerization catalysts, but the performance of these catalysts under more extreme conditions has not been reported. In this study, we evaluate the stability of a SBA-15 supported Ni-POM-WD catalyst in the presence of possible feed stream contaminants, such as CO, H_2, and CH_4, that could be present in alkane dehydrogenation and shale gas valorization plant streams. Propylene dimerization rates over Ni-POM-WD/SBA-15 were unaffected when co-feeding H_2 and CH_4. However, propane formation was dominant when co-feeding H_2 through hydrogenation pathways, while CH_4 was inert in the reaction chemistry. Co-feeding CO resulted in an immediate drop in propylene conversion, which was fully restored after the removal of CO and applying thermal regeneration. Evaluation of the catalysts by ^{31}P NMR and energy dispersion x-ray (EDX) mapping after exposure to each of the impurities provided evidence of structural stability with the Ni^{2+} sites intact after reaction and with no sign of particle or Ni agglomeration.

1. Introduction

Light alkene oligomerization is an important step in upgrading small chain olefins to a wide range of value-added precursors for petrochemicals and fuel products [1,2]. The major processes to produce light olefins are steam cracking and fluid catalytic cracking (FCC) of alkanes and naphtha [3–7]. Along with producing ethylene and propylene, these processes are accompanied by byproducts and stream contaminants, such as methane (CH_4), light alkanes, hydrogen (H_2), nitrogen (N_2), hydrogen sulfide (H_2S), water (H_2O), carbon dioxide (CO_2), and carbon monoxide (CO) [7–13]. The rise in shale gas production in the United States has increased the production of natural gas liquids, which provide olefin feedstocks, such as ethylene, propylene, and butene [14,15]. Therefore, there is an increased interest for a direct integrated process for conversion of shale gas into liquid products through alkane dehydrogenation, followed by olefin oligomerization [16–18]. The process streams from the proposed shale gas upgrading technologies that are fed to the oligomerization unit can contain H_2, N_2, saturated hydrocarbons, H_2O, and a considerable amount of CH_4 [16,17]. Expensive separation processes are used to isolate the olefins from the undesired contaminants [12,13,19,20]. Alternatively, process costs can be considerably decreased with simplified separation units upstream [19], utilizing catalysts downstream that exhibit resistance to byproducts and impurities [21–23].

Ni-exchanged solid catalysts have received considerable attention for olefin oligomerization owing to their selectivity to oligomers compared to other transition metals (Zr, Ti, and Cr) that favor polymerization and their ability to be recycled compared to homogeneous analogs [21,23,24]. Specifically, Ni-based solid catalysts have been tested for ethylene oligomerization reactions at a wide range of reaction conditions, yielding C4–C10 + products at 20–300 °C and 0.4–40 bar and achieving 99% conversion [21,25]. Whereas, solid acid catalysts, for example zeolites, require at least 150–250 °C to oligomerize ethylene in the liquid phase, resulting in diesel products at high pressures above 30 bar and 200–220 °C and gasoline products at ambient pressure with undesired cracking reactions occurring at ~200 °C [22,26,27]. Ni-exchanged catalysts are synthesized on the supports that contain Brønsted acid sites that participate in side reactions such as cracking, aromatization,

* Corresponding author.
E-mail address: jhicks3@nd.edu (J.C. Hicks).
[1] Orcid Id: 0000-0002-5054-2874

https://doi.org/10.1016/j.apcata.2022.118914
Received 29 June 2022; Received in revised form 1 September 2022; Accepted 20 September 2022
Available online 18 October 2022

disproportionation, and isomerization. These side reactions lead to lower selectivities and catalyst deactivation, especially at high reaction temperatures (> 180 °C) [21,24,25,28]. Metal-organic-frameworks (MOFs) have been studied as promising supports for Ni catalysts due to their high selectivity [29–33]. For instance, Ni embedded on Al-MOF achieved ~89 % selectivity for 1-butene at ~99 % ethylene conversion [33]. The main advantage of MOFs is the versatility of the material, such as tunability of the pore structure, electronic effects of the ligands, and control over the nature of the Ni sites, such as Ni within the MOF framework or Ni tethered to MOF nodes [29–34]. MOFs have been reported to exhibit good stability in the presence of H_2, H_2S, H_2O, CH_4, CO, and CO_2 [31,35], but they but they often need added co-catalyst to achieve high conversions and are also unstable under high-temperature gas-phase oligomerization conditions [34–39].

In our previous work, we showed that a Wells–Dawson-type polyoxometalate can be effectively used as a platform to isolate Ni^{2+} sites (Ni-POM-WD), and Ni-POM-WD dispersed within the pores of SBA-15 (Ni-POM-WD/SBA-15) was active for ethylene and propylene oligomerization reactions without any co-catalyst [40,41]. Further, during ethylene oligomerization reactions, the formed butenes were only linear [40], and propylene oligomerization resulted in a high selectivity for linear dimers (> 76 %) [41]. In addition, the initial activity of Ni-POM-WD/SBA-15 could be restored after olefin oligomerization by a thermal treatment under helium at 300 °C. Moreover, the activation energy for ethylene and propylene dimerization were 41 kJ/mol and 44.5 kJ/mol, respectively, which is comparable to Ni^{2+} exchanged-zeolites [40,41]. Since the transition metal substituted POMs have been studied for shale gas conversion, particularly oxidative dehydrogenation of methane, ethane, and propane [42], we hypothesize that these materials should be stable in the presence of feed impurities. In this work, we investigate the performance of Ni-POM-WD/SBA-15 for propylene oligomerization in the presence of H_2, CO, and CH_4. We performed a series of experiments where the feed was modulated between a pure and contaminated feed to evaluate the catalyst response to the impurity and the ability of the catalyst to recover after the impurity was removed. We also performed post-reaction characterization such as transmission electron microscopy (TEM) imaging, energy dispersive X-ray spectroscopy (EDX) mapping, and ^{31}P nuclear magnetic resonance (NMR) to evaluate the structural stability of the Ni-POM-WD to the various contaminants.

2. Experimental

2.1. Catalyst preparation

The immobilized Ni-POM-WD/SBA-15 was synthesized following a procedure described in literature [40,43–46]. First, 100 g of $Na_2WO_4{\cdot}2H_2O$ (Alfa Aesar, 99.0–101.0 %) was fully dissolved under reflux in 350 mL of de-ionized water (18.2 MΩ). After that, 150 mL of phosphoric acid (Millipore Sigma, 85 %) was slowly added and stirred under reflux for 24 h. Next, the obtained solution was precipitated by adding 100 g of potassium chloride (BDH Chemicals, 99.0–100.5 %) at ambient temperature, and the crude precipitate was recovered by vacuum filtration. Then the crude mixture was recrystallized to obtain the α/β-$K_6P_2W_{18}O_{62}$ mixture. The pure α-$K_6P_2W_{18}O_{62}$ crystals were separated from α/β-$K_6P_2W_{18}O_{62}$ by sequential base degradation and re-acidification and then transformed into lacunary POM-WD ($K_{10}P_2W_{17}O_{61}$) by adding 1 M $KHCO_3$ to α-$K_6P_2W_{18}O_{62}$. Ni-POM-WD was synthesized by mixing a nickel source ($Ni(NO_3)_2{\bullet}6\ H_2O$, Alfa Aesar, 98 %) and lacunary POM-WD in water. The final Ni-POM-WD precipitate was obtained by filtration. Lastly, Ni-POM-WD was supported on SBA-15 by the incipient wetness impregnation technique to obtain 10 wt % of Ni-POM-WD/SBA-15. The SBA-15 material was synthesized by following the reported procedure [40,47,48]. Approximately 18 g of P123 (Sigma-Aldrich) was fully dissolved in a mixture of 99.5 g of hydrochloric acid (Millipore Sigma, 37 %) and 550 g of de-ionized water. Afterwards, 39.8 g of tetraethyl orthosilicate (Acros Organics, 98 %) was added to the mixture and stirred at 35 °C for 20 h and further at 80 °C for 24 h. The resulting solid was filtered and washed with ~1 L of de-ionized water. As-synthesized SBA-15 was dried at 60 °C overnight. Lastly, the SBA-15 was calcined by first heating at 200 °C at 1.2 °C/min with a hold time of 1 h, followed by heating at 550 °C at 1.2 °C/min with a hold time of 6 h. Before use, SBA-15 was dried under vacuum at 200 °C for 3 h.

2.2. Catalyst characterization

Nitrogen physisorption was conducted on a Quantachrome 2200e instrument. The samples were degassed at 200 ℃ for 12 h under vacuum before the measurements. The nitrogen physisorption was performed at 77 K controlled by liquid nitrogen.

Solid-state ^{31}P MAS NMR on Ni-POM-WD/SBA-15 before and after the reaction was performed using a JEOL ECX-300. The samples were packed in a 3.2 mm zirconia sample tube. The packed sample tube was subjected to the measurement under the spinning rate of 10 kHz.

Solution ^{31}P NMR on Ni-POM-WD as prepared and after exposure to different gases was performed on a Bruker AVANCE III HD 500 MHz Nanobay. The samples were dissolved in a mixture of water and D_2O with a 9:1 ratio.

Ni weight loading of the prepared Ni-POM-WD/SBA-15 was determined via inductively coupled plasma optical emission spectroscopy (ICP-OES) using a on Perkin Elmer Optima 8000 ICP-OES. Ni-POM-WD/SBA-15 sample was added to 0.8 M of KOH solution at room temperature with a ratio of 0.001 g sample/1 g base and stirred until the sample was fully dissolved. After that, the mixture was dissolved in 2 vol % HNO_3 aqueous solution with a ratio of 0.067 g mixture/1 g acid. An external calibration curve was prepared from the Ni standard solution (BDH, 100 μg/mL in 2 % HNO_3 matrix).

High-angle annular dark-field scanning transmission electron microscopy (HAADF-STEM) images and energy dispersive X-ray spectroscopy (EDX) elemental mapping on as prepared and spent Ni-POM-WD/SBA-15 were done using a Spectra 300 transmission electron microscope operated at 300 kV. Before analysis samples were dispersed in acetone using sonication and then drop cast onto a carbon-coated copper grid.

2.3. Propylene oligomerization reactions

Catalyst reactions were performed in a stainless steel fixed-bed reactor (i.d. = 6.35 mm) at 180 °C, 1.01 bara, and 30 mL/min total flowrate. The feed gases were purified by in-line moisture traps (Matheson). For each reaction run 200 mg of catalyst was pelletized, sieved to 150–250 μm particle size, and diluted by Davisil® silica (150–250 μm). Before each reaction, the catalyst was pre-treated with pure helium (Airgas, Ultra High Purity) at 300 ℃ for 12 h to remove water from the catalyst, then the reactor was cooled to the reaction temperature at 180 °C. Hydrogen (Airgas, Ultra High Purity), carbon monoxide (Airgas, 30 % in helium), and methane (Airgas, Ultra High Purity) were mixed with propylene (Airgas, polymer grade) and helium for co-feeding studies. The feed composition without impurities was 16.7 % propylene and 83.3 % helium. For the contaminants co-feeding experiments, 16.7 % propylene was mixed separately with 5 %, 3.3 %, and 16.7 % of carbon monoxide, hydrogen, and methane, respectively, and balanced with helium. The products from the reactor were analyzed by an SRI 8610 C GC-FID (MTX-Wax 15 m MXT-Alumina BOND/MAPD 30 m columns, Restek). The products were identified by external standards 1-hexene (Sigma-Aldrich, ≥99 %), trans-2-hexene (Acros Organics, >98 %), cis-2-hexene (Alfa-Aesar, 96 %), trans-3-hexene (TCI, ≥99 %), cis-3-hexene (TCI, ≥97 %), 2-methyl-2-pentene (TCI, ≥95 %), 2-methyl-1-pentene (Acros Organics, 99 %), 4-methyl-1-pentene (Thermo Scientific, ≥98 %), trans-4-methyl-2-pentene (TCI, ≥97 %), 3-methyl-1-pentene (TCI, >98 %), trans-3-methyl-2-pentene (TCI, >99 %), cis-3-methyl-2-pentene (TCI, ≥95 %) and 2,3-dimethyl-1-butene (TCI, ≥98 %).

3. Results and discussion

3.1. Catalyst physicochemical and structural properties

The results of the elemental analysis and N_2 physisorption for Ni-POM-WD/SBA-15 are provided in Table 1 and Fig. S1. N_2 physisorption results show that the structure of the SBA-15 was preserved after Ni-POM-WD immobilization. As expected, the surface area and total pore volume of the initial SBA-15 decreased after 10 wt % of Ni-POM-WD was loaded into the SBA-15 pores due to pore filling and blocking interconnected micropores with the Ni-POM-WD clusters [40,41].

Fig. 1a depicts the solid-state magic angle spinning (SS MAS) ^{31}P NMR of as prepared Ni-POM-WD/SBA-15. The observed phosphorous feature at − 21.6 ppm represents the internal phosphate positioned further from the substituted Ni site within the Ni-POM-WD structure. The same P feature is observed in SS MAS ^{31}P NMR of the SBA-15 supported Ni-POM-WD and unsupported Ni-POM-WD (Fig. 1b) powders, indicating the structure remains intact after immobilization [40].

Fig. 2 depicts the Ni EDX mapping and the corresponding HAADF STEM image, showing the high surface area, mesoporous structure of SBA-15 for dispersion of the Ni-POM-WD crystals. This observation is consistent with previously reported results for these materials, which enhances the accessibility of propylene to the Ni active sites under reaction conditions [40]. In addition, Fig. S2 shows W, P, K, Si, and O EDX maps of Ni-POM-WD/SBA-15.

3.2. Catalyst response to CO Co-feeding experiments

Carbon monoxide was initially studied as an impurity in the propylene feed stream. The off-gas stream from an FCC and the outlet stream of a steam cracking process can contain CO [12,49]. Specifically, CO was added to a feed stream of propylene diluted with helium (C_3H_6: He = 1: 5) to assess the stability of Ni-POM-WD/SBA-15 at 180 °C and 1.01 bara. As shown in Fig. 3, the propylene consumption rate as a function of the time-on-stream (TOS) is plotted with and without CO co-feeding with catalyst regeneration steps included between each cycle. The 1st cycle was performed without the addition of CO in order to directly compare the catalyst performance to subsequent experiments conducted in the presence of CO. The propylene consumption rate begins at the maximum value and deactivates as a function of TOS. After the 1st cycle, the catalyst was regenerated under helium flow at 300 °C for 12 h to remove the heavier oligomeric products, which was shown to be an effective regeneration procedure on Ni-POM-WD/SBA-15 after the oligomerization reaction and deactivation [40]. During the 2nd cycle (Fig. 3), CO was co-fed with propylene. Remarkably, the normalized propylene consumption rate significantly decreased, and no deactivation trajectory was observed as the propylene consumption rate remained at a steady-state value throughout the cycle. The residual propylene conversion observed with CO addition is associated with the background propylene oligomerization. As shown in Fig. S4, the support (SBA-15 without Ni sites) was used as a benchmark material, and a small propylene consumption rate at 180 °C and 1.01 bara was measured, which is associated with the reaction of propylene on the support. An empty reactor and a reactor loaded with the lacunary form of the Wells–Dawson POM supported in SBA-15 (Fig. S5) at the same reaction conditions both showed no propylene oligomerization activity. Therefore, the drastic decrease in propylene consumption indicates direct competition between CO and propylene for Ni sites, resulting in the complete titration of available Ni for the reaction. The adverse effect of CO co-feeding during olefin oligomerization reaction has been previously reported by Kimura et al. who showed that a NiO-SiO_2 catalyst did not have ethylene oligomerization activity after being exposed to CO [50]. The deactivation of Ni^{2+} sites due to CO exposure can be explained by the ability of Ni^{2+} cations to form complexes with O-containing species [51,52]. Ni-alkyl species can react with CO reversibly forming Ni-acyl sites that are inactive for C–C coupling [53]. In addition, as reported in Cai et al., the exposure of $NiSO_4$/ɣ-Al_2O_3 to CO at 500 °C lowered the valency of Ni^{2+} to Ni^{+} and Ni^{0}, which resulted in a complete loss of the catalyst activity [54]. In this work, the Ni-POM-WD/SBA-15 catalyst was successfully regenerated after CO exposure using the same process noted previously, with the initial maximum propylene consumption rate fully restored, as shown in the first half of the 3rd cycle (Fig. 3). The recovery of oligomerization activity after regeneration indicates that the Ni^{2+} sites in Ni-POM-WD/SBA-15 remain Ni^{2+} and are not reduced by the CO.

As depicted in Fig. 3, the 3rd cycle started with a CO-free feed. After 430 min, 5 % CO was subsequently added to the feed, which immediately resulted in negligible propylene conversion. After an additional 150 min, CO co-feeding was stopped, and the propylene consumption rate increased, aligning with the projected values from the deactivation trajectory. Lastly, the catalyst was regenerated for the third time. In the 4th cycle (Fig. 3), the propylene oligomerization over the regenerated Ni-POM-WD/SBA-15 was performed in the absence of CO. During this cycle, the propylene consumption rate was nearly restored to the initial maximum propylene consumption rates obtained from the fresh catalyst (1st cycle). This is in line with literature results showing the reactivity of NiO/SiO_2-Al_2O_3 after poisoning did not recover significantly after the removal of CO from the feed, but the catalyst was successfully regenerated by combustion of the adsorbed species [55].

The product distribution for propylene oligomerization of the fresh catalyst and regenerated catalyst without CO co-feeding, corresponding to the 1st, 3rd (partial), and 4th cycles, is given in Table 2 with only propylene dimers observed throughout 4 cycles. The product distribution remained relatively stable with TOS, and Table 2 represents the average of the products for the duration of the corresponding cycle. The product distribution for each cycle without CO remained unchanged. The main formed products were trans-2-hexene (~30 %), trans-3-hexene (~20 %), cis-2-hexene (~14 %), cis-3-hexene (~11.5 %), and trans-4-methyl-2-pentene (~11.5 %). Such product distribution can be explained by the Cossee–Arlman mechanism [23]. The high selectivity towards linear hexenes, ~80 %, suggests the preferred pathway for propylene dimerization is 1,2-insertion of the first propylene to the nickel site, which is followed by 2,1-insertion of the second propylene to the nickel-propyl site [23,56]. Moreover, the molar ratios of trans-2-hexene/cis-2-hexene and trans-3-hexene/cis-3-hexene without CO co-feeding are lower than the equilibrium ratios (Table S1). Agirrezabal-Telleria et al. also reported differences in the measured and equilibrium ratios of the hexene isomers [57].

During the CO co-feeding reactions, the main products were trans-3-hexene, trans-2-hexene, followed by trans-4-methyl-2-pentene, 1-hexene, and 2-methyl-2-pentene (Table 2). The product distribution of the background reaction, which is the propylene conversion over SBA-15, had a similar distribution of C6s, the main formed products were trans-3-hexene, trans-2-hexene, 1-hexene, 2-methyl-2-pentene, and trans-4-methyl-2-pentene (Table 3). Because the selectivity for the hexenes is similar during CO co-feeding with Ni-POM-WD/SBA-15 catalyst and SBA-15 only, the small but measured propylene consumption rate during the CO co-feeding experiments is associated with the background reactivity of propylene, and CO molecules fully blocked Ni active sites. Moreover, the TGA analysis showed no sign of coke

Table 1
Elemental analysis and nitrogen physisorption pore properties of Ni-POM-WD/SBA-15 and SBA-15.

Sample	Ni wt %	BET Surface Area (m^2/g)	BJH Adsorption Pore Diameter (Å)	Total Pore Volume (cm^3/g)
SBA-15	–	790	68	0.64
Ni-POM-WD/SBA-15	0.12	540	68	0.60

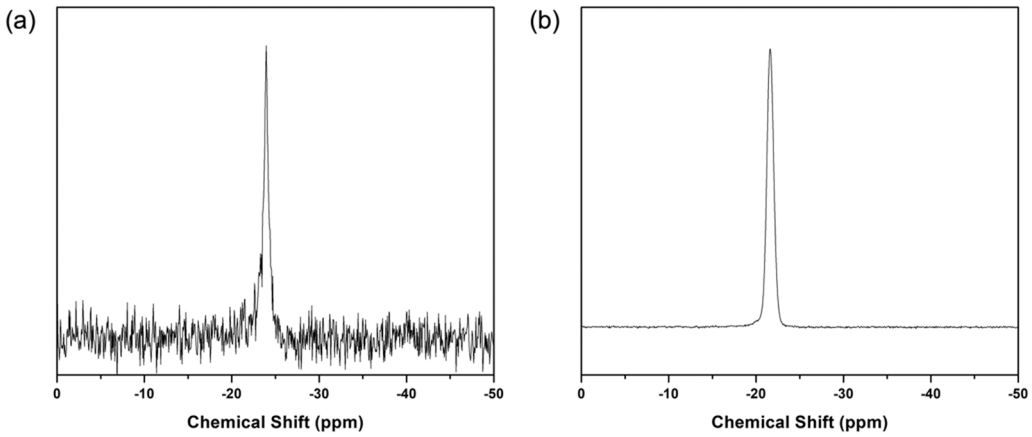

Fig. 1. Solid state MAS ^{31}P NMR of (a) fresh Ni-POM-WD/SBA-15 and (b) unsupported Ni-POM-WD.

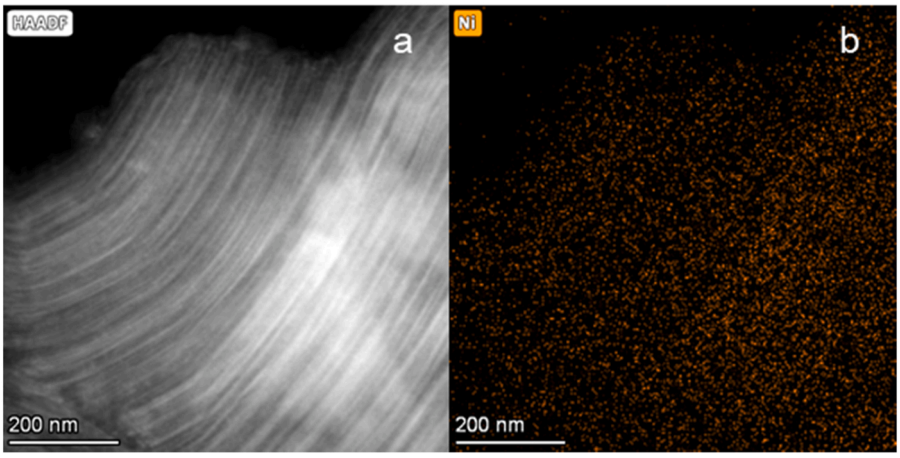

Fig. 2. HAADF STEM image (a) and Ni EDX map (b) of Ni-POM-WD/SBA-15.

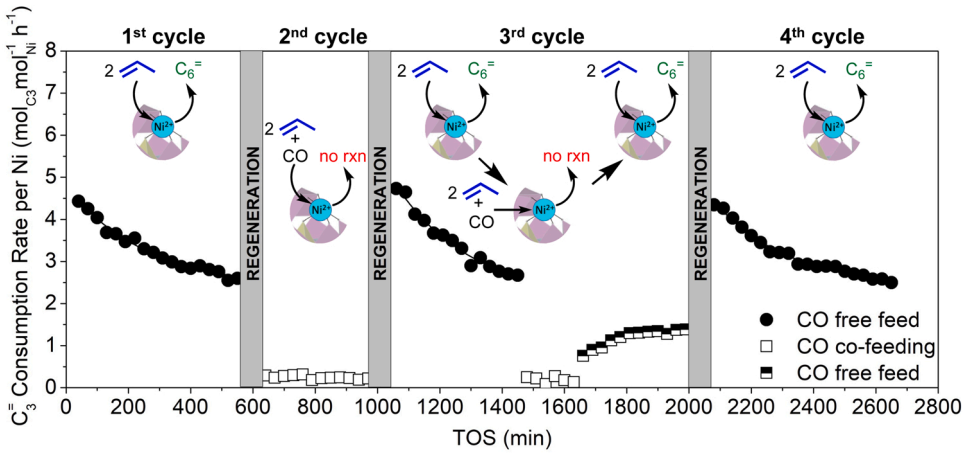

Fig. 3. Propylene consumption rate vs TOS in the presence of CO and CO free feed with regeneration in between cycles. The reaction is performed at 180 °C, 1.01 bara, 30 mL/min total flowrate, 16.7 % C_3H_6 + 83.3 % He or 16.7 % C_3H_6 + 5 % CO+ 78.3 % He.

formation (Fig. S11c).

The catalyst was characterized after the CO co-feeding experiments to further investigate the catalyst stability. From ^{31}P NMR (Fig. S3) results, no new NMR peaks or peak shifts were observed for Ni-POM-WD/SBA-15. Additionally, unsupported Ni-POM-WD exposed to CO under similar conditions also showed no change in the ^{31}P NMR spectrum. This shows that Ni sites remained intact with no signs of leaching from the POM structure. EDX mapping of Ni-POM-WD/SBA-15 after CO co-feeding was also performed (Fig. S9). The Ni, W, P, and K remain highly dispersed with no signs of particle agglomeration. Moreover, ICP analysis on spent catalyst provided no signs of Ni leaching, resulting in a similar Ni weight loading as the fresh Ni-POM-WD/SBA-15 (0.1 wt % Ni).

Table 2
The product distribution of propylene oligomerization on Ni-POM-WD/SBA-15 in the presence of CO and CO free feed with regeneration in between cycles. The reaction is performed at 180 °C, 1.01 bara, 30 mL/min total flowrate, 16.7 % C_3H_6 + 83.3 % He or 16.7 % C_3H_6 + 5 % CO+ 78.3 % He.

	1st cycle - no CO	2nd cycle - CO co-feed	3rd cycle - no CO	3rd cycle - CO co-feed	3rd cycle – no CO	4th cycle - no CO
	Average selectivity (%)					
trans-2-hexene	29.9	17.8	30.8	15.6	27.6	30.6
trans-3-hexene	20.2	37.1	19.5	35.8	21.6	19.7
cis-2-hexene	14.0	3.6	14.3	4.9	13.3	14.5
cis-3-hexene	11.5	0.7	11.7	0.0	11.1	11.6
1-hexene	4.4	13.3	4.1	16.2	5.8	4.4
trans-4-methyl-2-pentene	11.6	16.1	11.9	16.1	12.0	11.5
4-methyl-1-pentene	5.2	1.2	5.1	4.5	5.0	5.0
2-methyl-2-pentene	2.4	10.2	1.9	7.0	3.7	1.9
2,3-dimethyl-1-butene	0.8	0.0	0.8	0.0	0.0	0.7
Total linear hexenes	80.0	72.4	80.4	72.4	79.3	80.9

Table 3
The product distribution of propylene oligomerization on SBA-15. The reaction is performed at 180°C, 1.01 bara, 30 mL/min total flowrate, 16.7 % C_3H_6 + 83.3 % He.

	Average selectivity of C6 products (%)
trans-2-hexene	11.9
trans-3-hexene	49.8
cis-2-hexene	3.4
cis-3-hexene	2.2
1-hexene	12.0
trans-4-methyl-2-pentene	5.8
4-methyl-1-pentene	5.8
2-methyl-2-pentene	9.0
2,3-dimethyl-1-butene	0
Total linear hexenes	79.4

3.3. Catalyst performance evaluation in the presence of H_2/propylene mixtures

The performance of the Ni-POM-WD/SBA-15 propylene oligomerization catalyst was evaluated in presence of H_2. FCC off gas contains significant amount of H_2, 5–20 wt % [12]. Moreover, H_2 is produced along with propylene in the catalytic propane dehydrogenation process [58,59], and can be a byproduct from the direct shale gas upgrading plant after the alkane dehydrogenation step [16,19]. A complete separation of the alkenes from H_2 might not be possible, therefore, some amount of H_2 could be present in the oligomerization units [16]. Fig. 4 depicts the propylene consumption and propylene dimerization rates with respect to TOS. In these experiments, the Ni-POM-WD/SBA-15 was tested in a dilute propylene feed (C_3H_6: He = 1: 5) with and without H_2 co-feeding (H_2: C_3H_6 = 1: 10) at 180 °C and 1.01 bara total pressure. In the 1st cycle, the fresh catalyst was tested in the absence of H_2 in the feed. After 340 min, the catalyst was regenerated at 300 °C with helium, and subsequently tested with H_2 present in the feed (the 2nd cycle). In the last cycle, after the second thermal regeneration, the catalyst was tested in the 3rd cycle without H_2 co-feeding.

As shown in Fig. 4a, during the 1st cycle, the catalyst was tested in the absence of H_2 in the feed, and the propylene consumption rate followed identical trajectory as the fresh catalyst in Fig. 3. The propylene consumption rate with H_2 co-feed increased more than twice compared to the fresh catalyst cycle without H_2 co-feed, as shown in Fig. 4a. The increased propylene consumption rate is due to the propylene to propane hydrogenation reaction. The deactivation of the catalyst was associated with the heavy product build-up since the oligomerization reactions still occurred during propylene and H_2 co-feeding. After exposing Ni-POM-WD/SBA-15 to H_2 co-feeding, the catalyst was regenerated at 300 °C overnight with helium, and the subsequent propylene oligomerization rate without H_2 co-feeding resulted in full recovery of the catalyst as its initial activity. Co-feeding H_2 resulted in a slight decrease in hexene production rate (Fig. 4b), possibly due to some of the sites previously catalyzing oligomerization now performing propylene hydrogenation reactions. As a control experiment, the lacunary form of the Wells–Dawson POM showed no activity for propylene conversion in the presence of H_2 (Fig. S6).

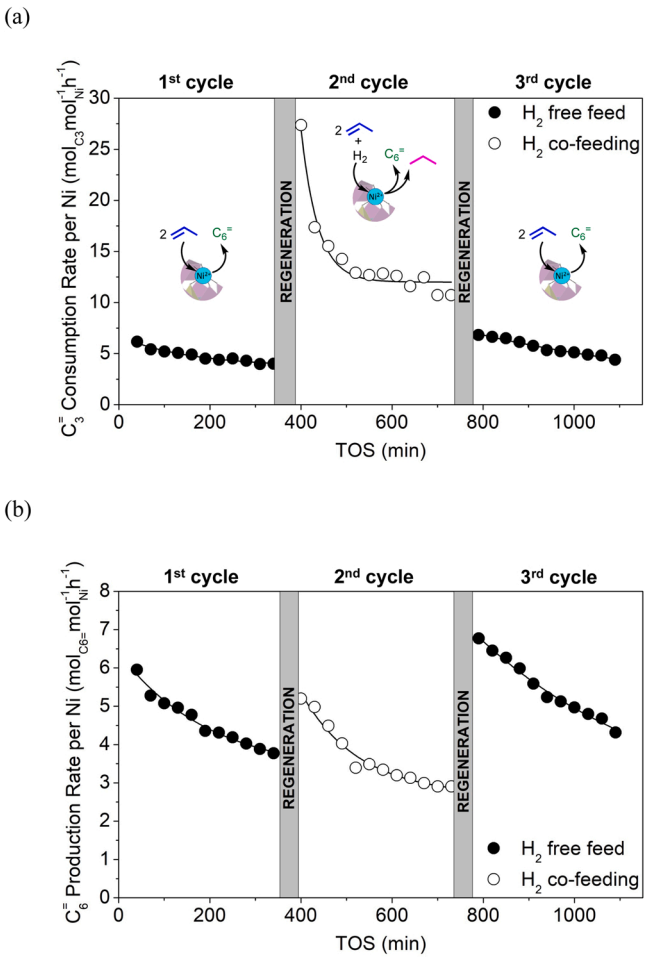

Fig. 4. Propylene consumption rate (a) and C6 production rate (b) vs TOS in the absence and with H_2 in the feed with regeneration in between cycles. The reaction is performed at 180 °C, 1.01 bara, 30 mL/min total flowrate, 16.7 % C_3H_6 + 83.3 % He or 16.7 % C_3H_6 + 3.3 % H_2 + 80 % He.

One of the proposed mechanisms for olefin oligomerization over Ni-based catalysts is the Cossee–Arlman pathway, which involves the formation of nickel-hydride intermediate species [60–63]. The olefin coordinates with a metal site, and another olefin inserts on the formed metal-carbon species [64,65]. The product desorbs via ß-hydride elimination or ß-hydride transfer, resulting in the formation of metal-H or metal-olefin-H [64,65]. A few studies have been performed to provide evidence on the formation mechanism of Ni-hydride sites on Ni-zeolite catalysts and proposed Ni-H as active sites [66,67], including

co-feeding H_2 during ethylene oligomerization [28]. Joshi et al. found that the activation period of butene site-time yield disappeared in the presence of H_2 on Ni-Li-[Al]Beta, which usually is present at the beginning of the reaction without H_2 in the feed [28]. The authors suggested H_2 in the feed reacts with Ni^{2+} sites and promotes the formation of active intermediate $[Ni(II)-H]^+$ sites [28]. They also observed the production of ethane from ethylene hydrogenation, acknowledging that Ni-hydride sites can catalyze alkene hydrogenation reactions. For Ni^{2+} sites in Ni-POM-WD/SBA-15, we observe similar reaction trends to Ni-zeolite catalysts, which may point to the formation of similar active sites that participate in simultaneous propylene oligomerization and hydrogenation reactions. However, the activation period on Ni-POM-WD/SBA-15 has not been observed with or without H_2 co-feeding and possibly observable in early TOS data.

The oligomerization product selectivity throughout all three reaction cycles was unchanged, and without H_2 in the feed, the selectivity was 100 % for propylene dimers (Table 4). During H_2 co-feeding cycle, the propane selectivity was 73.3 % and C6 olefins selectivity was 26.7 %. At the tested reaction conditions, saturated C6s were not observed, which is consistent with similar studies [28,68,69]. The distribution of the C6 products between all three cycles was invariant, which could imply that the literature proposed Ni-H active sites might be formed in-situ without H_2 co-feeding and during H_2 co-feeding. Moreover, no activation period at the onset of the reaction was observed on Ni-POM-WD, which indicates (1) that the active Ni-H sites are already present in the catalyst [28,68], (2) the active sites are formed from the Ni-alkyl intermediates [67], or (3) the activation period is very rapid and not captured in the initial TOS data.

The SS MAS ^{31}P NMR of Ni-POM-WD/SBA-15 after the reaction with H_2 co-feeding showed no change in features relative to the fresh catalyst (Fig. S7a). Additionally, the solution ^{31}P NMR of Ni-POM-WD crystals, which were exposed to pure H_2 at 180 °C for 2 h (Fig. S7b), did not indicate the degradation of the POM structure or Ni leaving the POMs. Similarly, EDX mapping showed no sign of aggregation of the POM or Ni (Fig. S9). These results highlight the structural stability of the Ni-POM-WD/SBA-15 to H_2, which is corroborated by the reaction results.

3.4. Catalyst evaluation in the presence of methane impurities

The behavior of Ni-POM-WD/SBA-15 for propylene oligomerization in the presence of CH_4 (CH_4: C_3H_6 = 1:1) was evaluated at 180 °C and 1.01 bara. Methane can be present in the olefin oligomerization feed if shale gas is directly used to produce oligomers [16]. The propylene consumption rate is shown in Fig. 5, where three reaction cycles with regeneration in between the cycles is provided. The regeneration

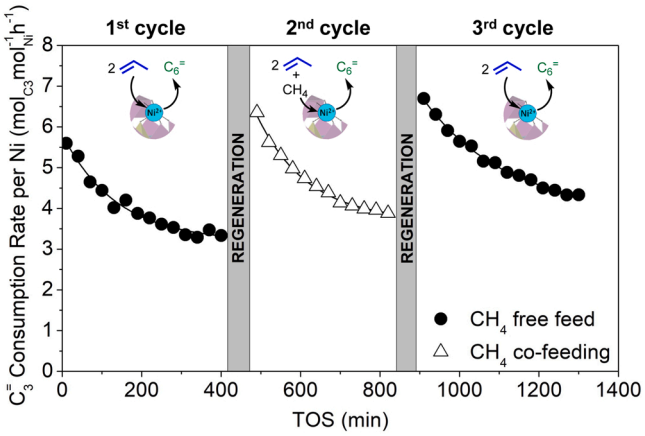

Fig. 5. Propylene consumption rate vs TOS in the absence and with CH_4 in the feed with regeneration in between cycles. The reaction is performed at 180 °C, 1.01 bara, 30 mL/min total flowrate, 16.7 % C_3H_6 + 83.3 % He or 16.7 % C_3H_6 + 16.7 % CH_4 + 66.6 % He.

treatment was performed using the same method as in the previous experiments. The 1st cycle was conducted on a fresh catalyst (Fig. 5). The catalyst behavior was similar to the 1st cycles depicted in Fig. 3 and Fig. 4, which is starting at a maximum propylene consumption rate and undergoing deactivation. After the regeneration treatment, the catalyst was tested with propylene and CH_4 in the feed during the 2nd cycle (Fig. 5), and the consumption rate and the deactivation behavior remained unchanged. This implies that methane does not participate in the oligomerization reactions or impact the catalytic site of the Ni-POM-WD/SBA-15; methane simply acts as an inert gas under these conditions. Activation of methane is challenging due to the high bond strength of C–H bonds (~434 kJ/mol) [70]. With Ni-based catalysts, methane decomposition to CHx fragments and solid carbon formation can be observed with reduced Ni particles in a temperature range of 200–350 °C [71,72]. The ability to regenerate the Ni-POM-WD/SBA-15 catalyst with only He indicates no coke-like carbon deposits formed and blocked Ni sites in the presence of CH_4. In addition, the TGA analysis showed no sign of coke formation (Fig. S11d). The 2nd cycle had an identical deactivation profile to the 1st and 3rd cycles, which further indicates that the Ni^{2+} sites were not reduced. A slight enhancement of the propylene conversion during the 3rd cycle, compared to the 1st cycle, could be due to improved dispersion of the Ni-POM-WD within SBA-15 from the thermal effect of regeneration.

At the tested reaction conditions, only propylene dimers were

Table 4
The product distribution of propylene oligomerization on Ni-POM-WD/SBA-15 in the absence and with H_2 in the feed with regeneration in between cycles. The reaction is performed at 180 °C, 1.01 bara, 30 mL/min total flowrate, 16.7 % C_3H_6 + 83.3 % He or 16.7 % C_3H_6 + 3.3 % H_2 + 80 % He.

	1st cycle - no H_2	2nd cycle - H_2 co-feed	3rd cycle - no H_2
	Average selectivity of C6 products (%)		
trans-2-hexene	30.3	29.2	30.9
trans-3-hexene	20.6	21.4	20.5
cis-2-hexene	13.2	12.5	13.6
cis-3-hexene	10.8	10.5	10.9
1-hexene	4.5	5.0	4.4
trans-4-methyl-2-pentene	12.1	12.1	11.7
4-methyl-1-pentene	4.9	4.9	4.8
2-methyl-2-pentene	2.4	3.0	2.2
2,3-dimethyl-1-butene	1.2	1.4	1.0
Total linear hexenes	79.3	78.6	80.3
Propane selectivity	0	73.3	0
C6 selectivity	100	26.7	100

Table 5
The product distribution of propylene oligomerization on Ni-POM-WD/SBA-15 in the absence and with CH_4 in the stream with regeneration in between cycles. The reaction is performed at 180 °C, 1.01 bara, 30 mL/min total flowrate, 16.7 % C_3H_6 + 83.3 % He or 16.7 % C_3H_6 + 16.7 % CH_4 + 66.6 % He.

	1st cycle - no CH_4	2nd cycle – CH_4 co-feed	3rd cycle - no CH_4
	Average selectivity (%)		
trans-2-hexene	29.9	30.4	30.8
trans-3-hexene	20.5	20.2	20.0
cis-2-hexene	13.3	13.7	14.2
cis-3-hexene	10.9	11.1	11.4
1-hexene	4.6	4.5	4.4
trans-4-methyl-2-pentene	12.4	12.0	11.7
4-methyl-1-pentene	5.2	5.0	4.9
2-methyl-2-pentene	2.3	2.1	1.7
2,3-dimethyl-1-butene	1.0	0.9	1.0
Total linear hexenes	79.2	79.9	80.7

observed. The averaged selectivity for each identified product is given in Table 5, and it shows that all three cycles provide the same product distribution. Analysis of the Ni-POM-WD/SBA-15 after reaction with CH_4 co-feeding using EDX mapping again showed no agglomeration of Ni or other elements in the POM structure (Fig. S9). Moreover, the solution ^{31}P NMR of Ni-POM-WD crystals, which were exposed to pure CH_4 at 180 °C for 2 h (Fig. S8), remained unchanged, which implies no degradation of the POM structure or Ni leaving the POMs.

4. Conclusion

In this work, the stability of Ni-POM-WD/SBA-15 was evaluated in the presence of potential feed impurities that olefin oligomerization catalysts may encounter. Even though the oligomerization reaction was less favored in the presence of CO and H_2, the catalytic nature of active sites remained unaltered, and the dimerization rates could be fully restored with thermal treatment. Further, the high selectivity for linear products with these catalysts, even with the mixed feeds, is attractive for the production of detergents and lubricants. The indifference of Ni-POM-WD to methane co-feeding opens the possibility of using shale gas or other alkanes as inert diluents, such as ethane and propane, which can be present in the stream after alkane dehydrogenation. These results highlight the remarkable catalytic behavior and stability of Ni-substituted polyoxometalates and their potential application to industrial settings.

CRediT authorship contribution statement

Galiya Magazova: Conceptualization, Investigation, Validation, Methodology, Writing – original draft preparation **Yoonrae Cho**: Investigation, Writing – review & editing. **Jessica Muhlenkamp**: Investigation, Writing – review & editing. **Jason Hicks**: Conceptualization, Funding acquisition, Resources, Writing – review & editing, Supervision.

Declaration of Competing Interest

The authors declare that they have no known competing financial interests or personal relationships that could have appeared to influence the work reported in this paper.

Data Availability

Data will be made available on request.

Acknowledgments

This work was supported by the Engineering Research Centers Program of the National Science Foundation under NSF Cooperative Agreement no. EEC-1647722. The authors would also like to acknowledge the Notre Dame Integrated Imaging Facility, the Notre Dame Magnetic Resonance Research Center, and the Notre Dame Centre for Environmental Science and Technology for use of their facilities.

Appendix A. Supporting information

Supplementary data associated with this article can be found in the online version at doi:10.1016/j.apcata.2022.118914.

References

[1] H. Olivier-Bourbigou, P.A.R. Breuil, L. Magna, T. Michel, M.F. Espada Pastor, D. Delcroix, Chem. Rev. 120 (2020) 7919–7983.
[2] S. Vernuccio, E.E. Bickel, R. Gounder, L.J. Broadbelt, ACS Catal. 9 (2019) 8996–9008.
[3] T. Ren, M. Patel, K. Blok, Energy 31 (2006) 425–451.
[4] M.L. Neelis, M. Patel, D.J. Gielen, K. Blok, Resour. Conserv Recycl 45 (2005) 226–250.
[5] S.M. Sadrameli, Fuel 140 (2015).
[6] R. Diercks, J.D. Arndt, S. Freyer, R. Geier, O. Machhammer, J. Schwartze, M. Volland, Chem. Eng. Technol. 31 (2008) 631–637.
[7] C. Godínez, A.L. Cabanes, G. Víllora, Chem. Eng. Process.: Process.Intensif. 34 (1995) 459–468.
[8] M. Bajus, V. Veselú, P.A. Leclercq, J.A. Rijks, Ind. Eng. Chem. Prod. Res. Dev. 18 (1979) 30–37.
[9] M. Bajus, V. Veselý, P.A. Leclercq, J.A. Rijks, Ind. Eng. Chem. Prod. Res. Dev. 19 (1980) 556–563.
[10] I. Dhuyvetter, M.F. Reyniers, G.F. Froment, G.B. Marin, D. Viennet, Ind. Eng. Chem. Res 40 (2001) 4353–4362.
[11] J.A. Santiago, J.D. Francesconi, N.L. Moretti, Oil Gas. J. 81 (1983) 78–82.
[12] C.P. Nicholas, A. Bhattacharyya, D.E. Mackowiak, Process for Oligomerizing Dilute Ethylene, B2, US Pat. 8 (575) (2013) 410. B2.
[13] H.-K.C. Timken, B.-K. Chang, C.B. Campbell, A.M. Thomas, M.A. Fernandez, M. Sessions, Ethylene Oligomerization Process for Making Hydrocarbon Liquids, US10683460B2, 2015.
[14] U.R. Chaudhuri, Fundamentals of Petroleum and Petrochemical Engineering, CRC Press,, 2016.
[15] A. Al-Douri, D. Sengupta, M.M. El-Halwagi, J. Nat. Gas. Sci. Eng. 45 (2017) 436–455.
[16] T. Ridha, Y. Li, E. Gençer, J.J. Siirola, J.T. Miller, F.H. Ribeiro, R. Agrawal, Processes 6 (2018).
[17] Z. Chen, Y. Li, W.P. Oladipupo, E.A. Rodriguez Gil, G. Sawyer, R. Agrawal, Cell Rep. Phys. Sci. 2 (2021).
[18] M.A. Stadtherr, D.T. Allen, H.S. Ganesh, D.P. Dean, S. Vernuccio, T.F. Edgar, M. Baldea, L.J. Broadbelt, Ind. Eng. Chem. Res 59 (2020) 3109–3119.
[19] Z. Chen, R. Agrawal, ACS Sustain Chem. Eng. 9 (2021) 13893–13901.
[20] Y. Fujiyama, M.H. Al-Tayyar, C.F. Dean, A. Aitani, H.H. Redhwi, Stud. Surf. Sci. Catal. 166 (2007).
[21] A. Finiels, F. Fajula, V. Hulea, Catal. Sci. Technol. 4 (2014) 2412–2426.
[22] C.P. Nicholas, Appl. Catal. A Gen. 543 (2017) 82–97.
[23] J. Skupińska, Chem. Rev. 91 (1991) 613–648.
[24] R. Joshi, A. Saxena, R. Gounder, Catal. Sci. Technol. 10 (2020) 7101–7123.
[25] E. Koninckx, P.S.F. Mendes, J.W. Thybaut, L.J. Broadbelt, Appl. Catal. A Gen. 624 (2021).
[26] C.T. O'Connor, M. Kojima, Catal. Today 6 (1990) 329–349.
[27] O. Muraza, Ind Eng, Chem. Res 54 (2015) 781–789.
[28] R. Joshi, G. Zhang, T. Miller, R. Gounder, ACS Catal. 8 (2018) 11407–11422.
[29] L. Chen, Y. Jiang, H. Huo, J. Liu, Y. Li, C. Li, N. Zhang, J. Wang, Appl. Catal. A Gen. 594 (2020).
[30] A.N. Mlinar, B.K. Keitz, D. Gygi, E.D. Bloch, J.R. Long, A.T. Bell, ACS Catal. 4 (2014) 717–721.
[31] A.J. Howarth, Y. Liu, P. Li, Z. Li, T.C. Wang, J.T. Hupp, O.K. Farha, Nat. Rev. Mater. 1 (2016) 1–15.
[32] Y.S. Wei, M. Zhang, R. Zou, Q. Xu, Chem. Rev. 120 (2020) 12089–12174.
[33] A. Alzamly, M. Bakiro, S. Hussein Ahmed, L.A. Siddig, H.L. Nguyen, Coord. Chem. Rev. 462 (2022), 214522.
[34] J. Canivet, S. Aguado, Y. Schuurman, D. Farrusseng, J. Am. Chem. Soc. 135 (2013) 4195–4198.
[35] J. Liu, Y. Yang, T.A. Goetjen, J.T. Hupp, Energy Environ Sci (2022).
[36] R.J. Comito, E.D. Metzger, Z. Wu, G. Zhang, C.H. Hendon, J.T. Miller, M. Dincă, Organometallics 36 (2017) 1681–1683.
[37] U.S.F. Arrozi, V. Bon, C. Kutzscher, I. Senkovska, S. Kaskel, Dalton Trans. 48 (2019) 3415–3421.
[38] K. Kyogoku, C. Yamada, Y. Suzuki, S. Nishiyama, K. Fukumoto, H. Yamamoto, S. Indo, M. Sano, T. Miyake, J. Jpn. Pet. Inst. 53 (2010) 308–312.
[39] D. Yang, B.C. Gates, ACS Catal. 9 (2019) 1779–1798.
[40] Y. Cho, J.A. Muhlenkamp, A.G. Oliver, J.C. Hicks, Chem. Commun. 57 (2021) 13772–13775.
[41] G. Magazova, Y.C. Cho, J. Muhlenkamp, J.C. Hicks, Catal. Sci. Technol. (2022).
[42] M. Sun, J. Zhang, P. Putaj, V. Caps, F. Lefebvre, J. Pelletier, J.-M. Basset, Chem. Rev. 114 (2014) 981–1019.
[43] J.H. Choi, J.K. Kim, S. Park, J.H. Song, I.K. Song, Appl. Catal. A Gen. 427 428 (2012) 79–84.
[44] J.H. Choi, J.K. Kim, D.R. Park, T.H. Kang, J.H. Song, I.K. Song, J. Mol. Catal. A Chem. 371 (2013) 111–117.
[45] D.K. Lyon, W.K. Miller, T. Novet, P.J. Domaille, E. Evitt, D.C. Johnson, R.G. Finke, J. Am. Chem. Soc. 113 (1991) 7209–7221.
[46] B.J. Hornstein, R.G. Finke, Inorg. Chem. 41 (2002) 2720–2730.
[47] D. Zhao, J. Feng, Q. Huo, N. Melosh, G.H. Fredrickson, B.F. Chmelka, G.D. Stucky, Science 279 (1998) (1979) 548–552.
[48] J.C. Hicks, B.A. Mullis, C.W. Jones, J. Am. Chem. Soc. 129 (2007) 8426–8427.
[49] S. Seifzadeh Haghighi, M.R. Rahimpour, S. Raeissi, O. Dehghani, Chem. Eng. J. 228 (2013) 1158–1167.
[50] K. Kimura, H. A-I, A. Ozaki, J. Catal. 18 (1970) 271–280.
[51] R.D. Andrei, E. Borodina, D. Minoux, N. Nesterenko, J. Dath, C. Cammarano, V. Hulea, Ind. Eng. Chem. Res 59 (2020) 1746–1752.
[52] L. Bonneviot, D. Olivier, M. Che, J. Mol. Catal. 21 (1983) 415–430.
[53] E. Carmona, F. González, M.L. Poveda, J.L. Atwood, R.D. Rogers, J. Chem. Soc., Dalton Trans. (1980).
[54] T. Cai, D. Cao, Z. Song, L. Li, Appl. Catal. A Gen. 95 (1993) L1–L7.
[55] J.P. Hogan, R.L. Banks, W.C. Lanning, A. Clark, Ind. Eng. Chem. 47 (1955).
[56] A.N. Mlinar, O.C. Ho, G.G. Bong, A.T. Bell, ChemCatChem 5 (2013) 3139–3147.

[57] I. Agirrezabal-Telleria, E. Iglesia, J. Catal. 389 (2020) 690–705.
[58] S. Chen, X. Chang, G. Sun, T. Zhang, Y. Xu, Y. Wang, C. Pei, J. Gong, Chem. Soc. Rev. 50 (2021) 3315–3354.
[59] A. Agarwal, D. Sengupta, M. El-Halwagi, A.C.S. Sustain, Chem. Eng. 6 (2018) 2407–2421.
[60] F.X. Cai, C. Lepetit, M. Kermarec, D. Olivier, J. Mol. Catal. 43 (1987) 93–116.
[61] K. Toch, J.W. Thybaut, G.B. Marin, Appl. Catal. A Gen. 489 (2015) 292–304.
[62] R. Henry, M. Komurcu, Y. Ganjkhanlou, R.Y. Brogaard, L. Lu, K.J. Jens, G. Berlier, U. Olsbye, Catal. Today 299 (2018) 154–163.
[63] S. Forget, H. Olivier-Bourbigou, D. Delcroix, ChemCatChem 9 (2017) 2408–2417.
[64] P. Cossee, J. Catal. 3 (1964) 80–88.
[65] E.J. Arlman, P. Cossee, J. Catal. 3 (1964) 99–104.
[66] S. Moussa, P. Concepcio, A. Arribas, ACS Catal. 8 (2018) 3903–3912.
[67] R.Y. Brogaard, U. Olsbye, ACS Catal. 6 (2016) 1205–1214.
[68] A. Saxena, R. Joshi, R.R. Seemakurthi, E. Koninckx, L.J. Broadbelt, J. Greeley, R. Gounder, ACS Eng. Au 2 (2022) 12–16.
[69] D.L. Trimm, I.O.Y. Liu, N.W. Cant, Appl. Catal. A Gen. 374 (2010) 58–64.
[70] X. Guo, G. Fang, G. Li, H. Ma, H. Fan, L. Yu, C. Ma, X. Wu, D. Deng, M. Wei, D. Tan, R. Si, S. Zhang, J. Li, L. Sun, Z. Tang, X. Pan, X. Bao, Science 344 (1979) 616–619, 2014.
[71] J. Guo, H. Lou, X. Zheng, Carbon N. Y 45 (2007) 1314–1321.
[72] W. Gac, A. Denis, T. Borowiecki, L. Kepiński, Appl. Catal. A Gen. 357 (2009) 236–243.